JACS
JOURNAL OF THE AMERICAN CHEMICAL SOCIETY
Article
pubs.acs.org/JACS

Spatially Organized Enzymes Drive Cofactor-Coupled Cascade Reactions

Tien Anh Ngo, Eiji Nakata, Masayuki Saimura, and Takashi Morii*

Institute of Advanced Energy, Kyoto University, Uji, Kyoto 611-0011, Japan

Supporting Information

ABSTRACT: We report the construction of an artificial enzyme cascade based on the xylose metabolic pathway. Two enzymes, xylose reductase and xylitol dehydrogenase, were assembled at specific locations on DNA origami by using DNA-binding protein adaptors with systematic variations in the interenzyme distances and defined numbers of enzyme molecules. The reaction system, which localized the two enzymes in close proximity to facilitate transport of reaction intermediates, resulted in significantly higher yields of the conversion of xylose into xylulose through the intermediate xylitol with recycling of the cofactor NADH. Analysis of the initial reaction rate, regenerated amount of NADH, and simulation of the intermediates' diffusion indicated that the intermediates diffused to the second enzyme by Brownian motion. The efficiency of the cascade reaction with the bimolecular transport of xylitol and NAD^+ likely depends more on the interenzyme distance than that of the cascade reaction with unimolecular transport between two enzymes.

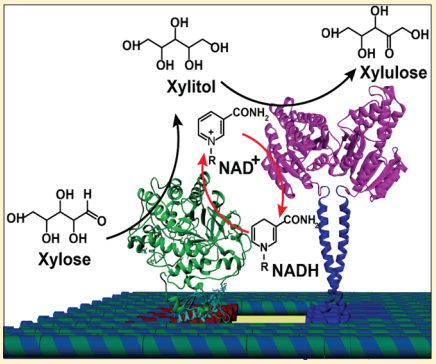

INTRODUCTION

In cellular enzyme cascades, efficient transport of an intermediate is often driven by confining free diffusion in a compartment of spatially organized enzymes.[1−14] When the enzymes are in close proximity to each other upon compartmentalization in the cell, the formation of byproducts is substantially reduced, leading to high turnover and obstructive effects, such as inhibition of the final product, and unfavorable kinetics can be reduced.[11,12] In the typical substrate channeling mechanism observed in nature, the intermediate from the first enzyme is transported directly to the second enzyme without diffusion to the bulk phase to maximize the efficiency of sequential reactions. When enzymes are positioned near enough to each other such that the intermediate produced by the first enzyme is processed efficiently by the second enzyme before diffusing in bulk solution, a proximity effect is expected to enhance the sequential reaction. In order to understand the role of the spatial organization of enzymes, enzyme cascade reactions have been studied in vitro or in cell by immobilizing enzymes on the scaffold, such as proteins,[15−17] lipid bilayer,[18] and nucleic acids.[19−21] Though simulation studies indicated that the substrate channeling including proximity channeling would be observed within 1 nm of interenzyme distance,[22−27] experimental results indicated that the enzyme cascade reactions were enhanced for the systems with the interenzyme distance of more than 1 nm.[28−31] Thus, a question whether the efficient transport of an intermediate is governed by its simple diffusion or not remains to be clarified.[3,6,9,11−14] Additionally, the mechanism of the intermediate transport between two enzymes would become more crucial when more than one molecule, such as the intermediate and a cofactor, are involved in the enzyme cascade reaction.

Recently, DNA nanostructures[32−34] have been applied as scaffolds for the spatial organization of enzymes to form artificial enzyme cascades with which the efficient transport of reaction intermediates can be modeled.[28−31,35,36] The definable nature of DNA nanostructures allows for the construction of a variety of spatially constrained enzyme assemblies, such as glucose oxidase/horseradish peroxidase[28−31] or glucose-6-phsphate dehydrogenase/malic dehydrogenase,[35] thus supporting their use as ideal scaffolds for this purpose.[37] Site-specific attachment of enzymes on the DNA scaffold was mostly carried out by tethering of the enzymes through oligodeoxynucleotides (ODNs).[28−31,35,38] One drawback of this method is that the activity of the enzymes attached to the ODNs tends to decrease compared with the activity of native enzymes.[28,29,31,35] Therefore, to overcome this problem, we developed methods to use sequence-specific DNA-binding proteins, the zinc finger protein (zif268)[39] and the basic leucine-zipper protein (GCN4),[40] as adaptors to stably locate the enzymes at specific positions on the DNA origami scaffold.[41,42] Our protein-adaptor-based method successfully assembled the recombinant enzymes in high loading yields with control of the number of enzyme molecules and maintenance of the catalytic activities of enzymes.

Here, we report the construction of an artificial enzyme cascade based on the D-xylose metabolic pathway. D-Xylose is a five-carbon aldose that can be metabolized into useful products

Received: September 29, 2015
Published: February 16, 2016

DOI: 10.1021/jacs.5b10198
J. Am. Chem. Soc. 2016, 138, 3012−3021

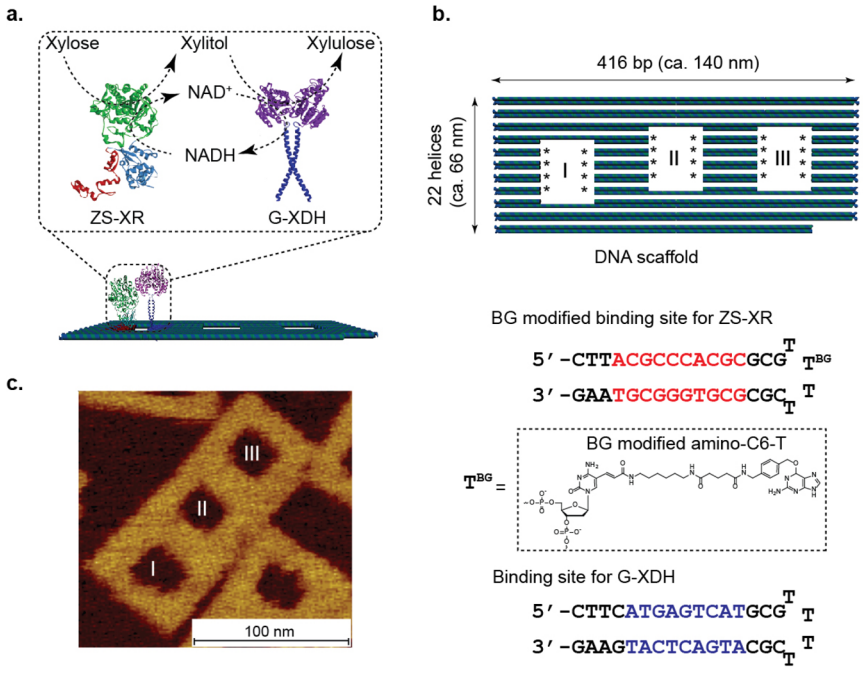

Figure 1. Design of the adaptor-fused enzymes and DNA origami scaffolds. (a) Schematic illustration of the enzymatic cascade reactions by the coassembled enzymes ZS-XR and G-XDH on the DNA scaffold. (b) Illustration of the DNA origami scaffold (top) showing the three cavities (I, II, and III), each of which held up to eight hairpin DNAs containing the specific binding sites for either ZS-XR (middle) or G-XDH (bottom) at the positions indicated by asterisks. The chemical structure of BG-modified thymine, denoted as "T^{BG}", is shown. (c) An AFM image of the designed DNA scaffold without incorporation of the target hairpin DNA for the enzyme inside the cavities.

by a variety of organisms.[43] In addition to its biological significance, D-xylose is a major product of the hydrolysis of lignocellulosic biomass, which can be fermented to bioethanol or biohydrogen by bacteria, yeasts, and filamentous fungi.[43−45] Within the metabolic pathway of xylose, we have focused on the oxidoreductase pathway,[45] also called the xylose reductase (XR)−xylitol dehydrogenase (XDH) pathway. In the artificially designed cascade, the first enzyme XR converts xylose into xylitol by consuming the cofactor NADH. The produced xylitol and NAD^+ are both simultaneously transported to the second enzyme XDH, which converts xylitol into xylulose by consuming NAD^+ to recycle the NADH cofactor (Figure 1a). DNA origami[33] was utilized as a scaffold to coassemble the enzymes XR and XDH in this artificial D-xylose metabolic pathway. The enzyme coassembly formed as designed through the protein-based adaptors, with variations in the interenzyme distance and defined numbers of enzyme molecules. We systematically evaluated the sequential reactions of xylose metabolism through the simultaneous bimolecular transport of xylitol and NAD^+ from XR to XDH with recycling of the cofactor NADH. The efficiency of the cascade reaction was highly dependent on the interenzyme distance between XR and XDH.

RESULTS

Construction of Adaptor-Fused Enzymes. A mutant of XR and native XDH derived from *Pichia stipitis*, both of which have been applied in a recombinant *Saccharomyces cerevisiae* mutant to convert xylose to ethanol,[46,47] were utilized to build the artificial metabolic cascade to yield xylulose from xylose through xylitol in vitro (Figure 1a). In *P. stipitis*, NADPH is oxidized into $NADP^+$ by native XR; however, NAD^+ is the preferential cofactor over $NADP^+$ for XDH.[46] Thus, a mutant XR with a preference for NADH was used to recycle NADH during the sequential enzymatic reactions.

To specifically locate XDH on the DNA scaffold, XDH was fused to the C-terminus of the GCN4 adaptor through a Gly-Gly-Ser linker to give G-XDH (Figure 1a and Figure S1b in the Supporting Information) as reported previously. The resulting G-XDH formed homodimers, and its ability to convert xylitol into xylulose in the presence of NAD^+ was higher than that of the native XDH in bulk solution.[42] The mutant XR was orthogonally localized to a specific position on the DNA scaffold by applying a modular adaptor (ZS)[48] consisting of both the DNA-binding zif268 protein[39] and a cross-link-forming SNAP-tag[49] (Figure 1a and Figures S1a and S2 in the Supporting Information). In the modular adaptor-fused enzyme ZS-XR, zif268 bound to the specific DNA sequence placed in the DNA scaffold, whereas the SNAP-tag formed a covalent linkage with benzylguanine (BG) incorporated in the target DNA sequence.[48] With this setup the mutant XR could be placed at the desired position in high yield. ZS-XR exhibited higher enzymatic activity than the mutant XR, with k_{cat}/K_m values of $(11 \pm 0.8) \times 10^6$ and $(6 \pm 0.7) \times 10^6$ M^{-1} s^{-1}, respectively, in bulk solution (Figure S3 and Table S1 in the Supporting Information).

Binding of the Adaptor-Conjugated Enzymes to DNA Scaffolds. To assemble the enzymes on the scaffold, we designed a DNA origami with three rectangular cavities (namely, cavities I, II, and III), in which the hairpin DNAs containing the target sequences for the adaptors were placed. Each cavity held up to eight binding sites for ZS-XR with the BG modification and/or for G-XDH (Figure 1b,c and Figure S4 and Tables S10−12 in the Supporting Information). The DNA origami was prepared as described[33] and the enzyme−DNA scaffold was purified by gel filtration to remove the unbound

DOI: 10.1021/jacs.5b10198
J. Am. Chem. Soc. 2016, 138, 3012−3021

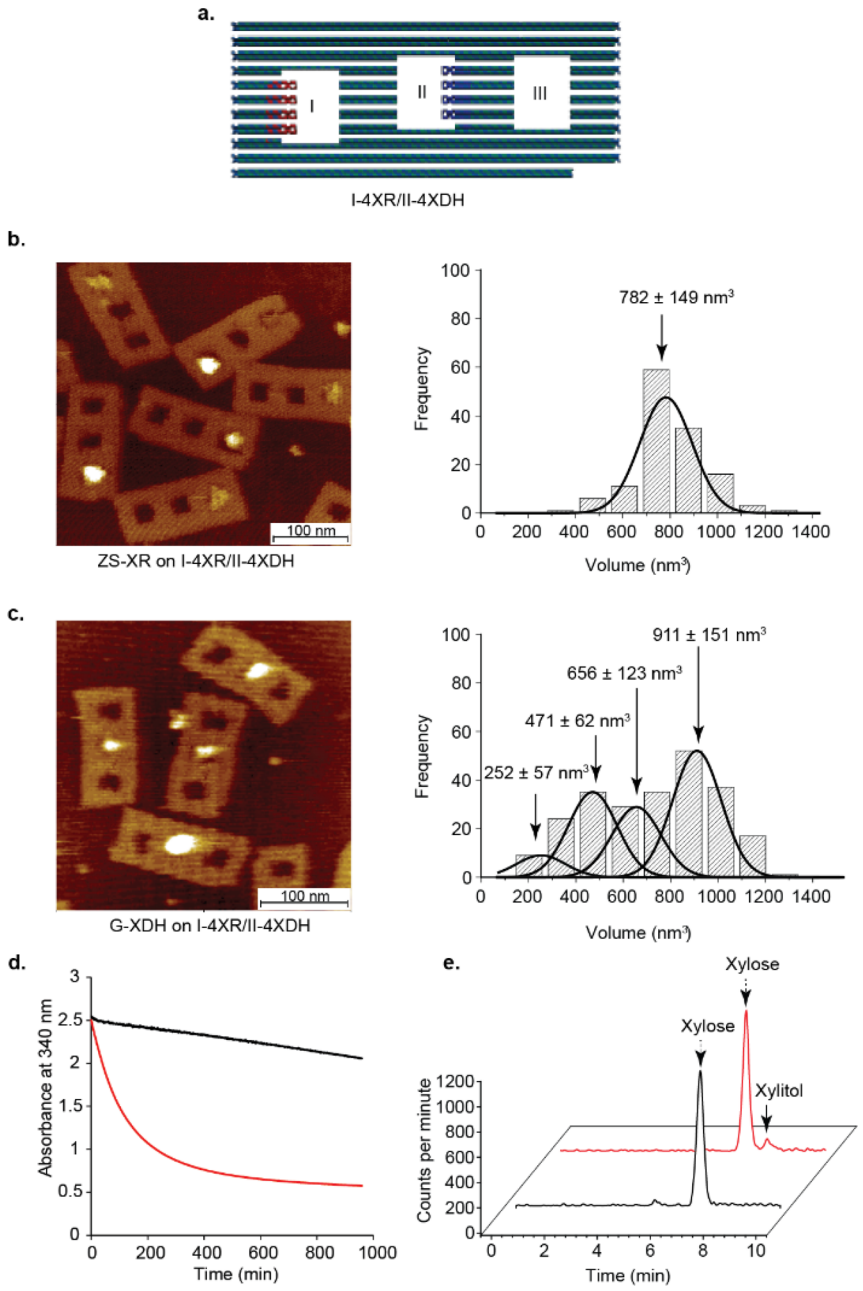

Figure 2. Enzyme assemblies and catalytic activities on the DNA scaffold. (a) Illustration of the DNA scaffold (I-4XR/II-4XDH) containing a set of four binding sites for each ZS-XR (red) in cavity I and G-XDH (blue) in cavity II. (b, c) AFM images (left) and protein volume analysis (right) of (b) ZS-XR or (c) G-XDH bound to the DNA scaffold (I-4XR/II-4XDH). The frequency distributions of the molecular volumes of (b, right) ZS-XR (n = 132) and (c, right) G-XDH (n = 239) bound in cavities I and II of I-4XR/II-4XDH, respectively, are shown. [I-4XR/II-4XDH] = 13.6 nM and [ZS-XR] and [G-XDH] = 300 nM. The reactions were carried out for 30 min on ice. (d) The catalytic activity of ZS-XR (red line) loaded on a DNA scaffold containing four binding sites for ZS-XR inside cavity I (I-4XR) was measured by determining time-dependent changes in absorbance at 340 nm. The black line indicates the control sample without ZS-XR. (e) HPLC chromatograms of the reaction mixture of ZS-XR on I-4XR with [1-^{3}H]xylose before (black line) or after (red line) a 16-h incubation. Experimental conditions are shown in the Materials and Methods.

enzymes. For the detailed experimental procedure, see the Materials and Methods.

The DNA scaffold was designed to have four binding sites for ZS-XR with the BG modification inside cavity I and four binding sites for G-XDH inside cavity II (I-4XR/II-4XDH; Figure 2a). The atomic force microscopy (AFM) images of the DNA scaffold assembled with ZS-XR or G-XDH indicated that 95% of cavity I and 78% of cavity II were occupied by ZS-XR or G-XDH, respectively, while less than 10% of enzymes were found to nonspecifically interact with other regions of the DNA scaffold (Figure 2b,c and Table S2 in the Supporting Information). The actual number of enzymes bound to the target sites was assessed using volume analysis of enzymes in the AFM image[48] (Figure 2b,c, right, and Note S2 and Figures S6 and S7 in the Supporting Information). For the assemblies with ZS-XR, a single peak corresponding to four ZS-XR molecules (Figure 2b, right) was observed for cavity I. The formation of the covalent linkage was quite effective for loading the expected four molecules of ZS-XR at the predesigned positions inside the cavity. The DNA scaffold treated with G-

DOI: 10.1021/jacs.5b10198
J. Am. Chem. Soc. 2016, 138, 3012−3021

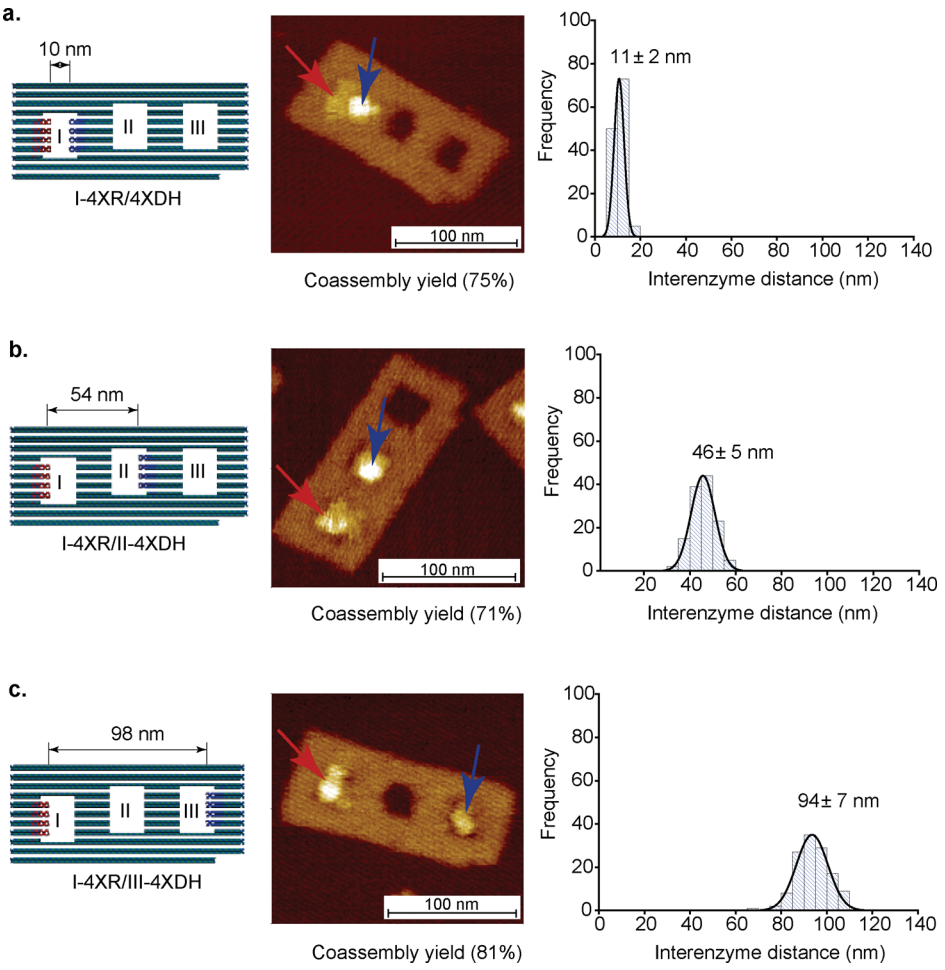

Figure 3. Distance-dependent coassembly of enzymes inside the cavity of the DNA scaffold and analysis of the interenzyme distance. (Left) Illustrations of the DNA scaffold containing a set of four binding sites for ZS-XR (red) and G-XDH (blue). These designs yielded interenzyme distances of 10, 54, and 98 nm, respectively, for (a) I-4XR/4XDH, (b) I-4XR/II-4XDH, and (c) I-4XR/III-4XDH. (Middle) AFM images of the DNA scaffold with bound enzymes. The red and blue arrows indicate ZS-XR and G-XDH, respectively. (Right) Statistical analyses of the observed interenzyme distances (center-to-center) between ZS-XR and G-XDH. [DNA scaffold] = 13.6 nM, [ZS-XR] = 300 nM, and [G-XDH] = 300 nM. Reactions were carried out for 30 min on ice.

XDH exhibited frequency distributions covering a broad range of volumes corresponding to two (7%), four (28%), six (23%), and eight (42%) monomers of G-XDH in cavity II (Figure 2c, right). On average, 4.7 G-XDH monomers were loaded in cavity II (Note S2 in the Supporting Information).

Activities of the Enzymes Loaded in the Cavities of the DNA Scaffold. The enzymatic activity of covalently loaded ZS-XR inside the cavities within the DNA scaffold was assessed by measuring the oxidation of NADH spectrophotometrically at 340 nm and by monitoring the production of xylitol using high-performance liquid chromatography (HPLC) analyses. A DNA scaffold possessing four binding sites for ZS-XR in cavity I (I-4XR, Figure S8a in the Supporting Information) was covalently assembled with ZS-XR and then purified by gel filtration to remove the unbound enzyme before the enzymatic assay. The AFM images indicated that binding of ZS-XR occurred inside cavity I as designed, with a yield of 97% (Figure S8b and Table S2 in the Supporting Information). The actual number of ZS-XR molecules in the cavity was estimated to be four, as assessed by volume analyses (Figure S8c in the Supporting Information). Time-dependent changes in NADH oxidation revealed that the reaction with ZS-XR on the DNA scaffold (21 nM) yielded 1287 ± 218 μM NAD^+ after 16 h of incubation at 25 °C (Figure 2d). The amount of xylitol produced by reaction with [1-^{3}H]xylose was 904 ± 152 μM (Figure 2e). The enzymatic activity of covalently loaded ZS-XR on the DNA scaffold was unaffected (Figure S9 in the Supporting Information). The second enzyme G-XDH assembled on the DNA scaffold has previously been shown to be as active as the free enzyme.[42]

Construction of a Sequential Enzyme Cascade and the Analysis of Distance Dependency. We then coassembled both enzymes to form a sequential array of XR and XDH (Figure 1a). In this experiment, the DNA scaffold was designed to have four binding sites for each adaptor, such that four ZS-XR molecules and eight G-XDH molecules (i.e., four homodimers) could be stably integrated (Figure 3). Three different types of DNA scaffolds were prepared by placing a set of four hairpin DNA sequences with the binding sites for G-XDH at the right side of (i) cavity I, (ii) cavity II, and (iii) cavity III. Additionally, a set of four hairpin DNAs with binding sites for ZS-XR was placed at the left side of the inside of cavity I. This design produced interenzyme distances between ZS-XR and G-XDH of about 10, 54, and 98 nm when G-XDH was placed in cavities I, II, and III, respectively (Figure 3 and Figure S11 in the Supporting Information).

DOI: 10.1021/jacs.5b10198
J. Am. Chem. Soc. 2016, 138, 3012−3021

Enzymes were loaded onto these DNA scaffolds, and the binding was characterized by AFM imaging. The AFM images indicated that both of the enzymes were simultaneously located at the positions as designed, and the coassembly yields were 75%, 71%, and 81%, respectively, for the interenzyme distances of 10, 54, and 98 nm (Figure 3a–c, middle, and Figures S12–S14 in the Supporting Information). The actual number of coassembled enzymes was estimated by volume analyses (Figures S12–S14 in the Supporting Information). For all cases, four molecules of ZS-XR were found in cavity I, as designed. The average numbers of bound G-XDH monomers (Figure 4a) were 4.2, 3.8, and 4.4 in cavities I, II, and III, respectively. The interenzyme distances between ZS-XR and G-XDH were also estimated for each case from the AFM images and were 11 ± 2, 46 ± 5, and 94 ± 7 nm, consistent with the original designs (Figure 3a–c, right).

The sequential reactions were then examined by monitoring time-dependent changes in the absorbance at 340 nm, representing NADH. The reaction of the coassembled enzymes was started with the addition of NADH (2 mM) to a mixture of the substrate xylose (12.5 mM) and each ZS-XR assembly of DNA scaffold (I-4XR/4XDH, I-4XR/II-4XDH, or I-4XR/III-4XDH; 21 nM) in the presence of G-XDH (85 nM in the dimer form). During the course of the sequential enzymatic reactions (Figure 1a), the amount of NADH in the solution was equal to the total of NADH remaining after the first ZS-XR reaction and the NADH regenerated by the second enzyme G-XDH at any given point. To estimate the amount of NADH regenerated by the second enzymatic reaction as a measure of cascade reactions, the amount of remaining NADH after the first enzymatic reaction at a given time was subtracted from the total amount. For this purpose, a reaction of ZS-XR loaded on the DNA scaffold (I-4XR) was performed in the absence of G-XDH to estimate the amount of remaining NADH after the first enzymatic reaction. In addition, to compare the cascade reactions on the DNA scaffold with that of the free diffusion of the substrate in bulk solution, a reaction of ZS-XR loaded on the DNA scaffold I-4XR and free G-XDH was carried out. In this case, the intermediates xylitol and NAD^+ produced by ZS-XR on the DNA scaffold were freely diffused into the bulk solution, and the second step reaction, catalyzed by G-XDH, occurred in solution. On the basis of the concentrations of both of the enzymes, the interenzyme distance was theoretically estimated to be 249 nm (Note S3 in the Supporting Information).

The apparent consumption of NADH was confirmed by the decrease in absorption for all the reactions (Figure S15 in the Supporting Information). Upon subtraction of the remaining NADH after the first step, the ZS-XR reaction, the amount of regenerated NADH for each reaction was estimated and plotted over the reaction time, as given in Figure 4b. As expected, the amount of regenerated NADH increased as the interenzyme distance decreased and was much higher than that of the free diffusion system (ZS-XR on the DNA scaffold and free G-XDH in solution), indicating that the efficiency of the enzyme cascade reaction was actually enhanced on the coassembled systems.

The initial rate of NADH regeneration (V_{ini}) by G-XDH could be used as a measure of the efficiency of the cascade reaction.[8,28,50,51] This rate was obtained from the slope of the plot of the time-dependent regeneration of NADH for the free diffusion and enzyme coassembly systems (Figure 4b). Additionally, the amount of regenerated NADH was estimated

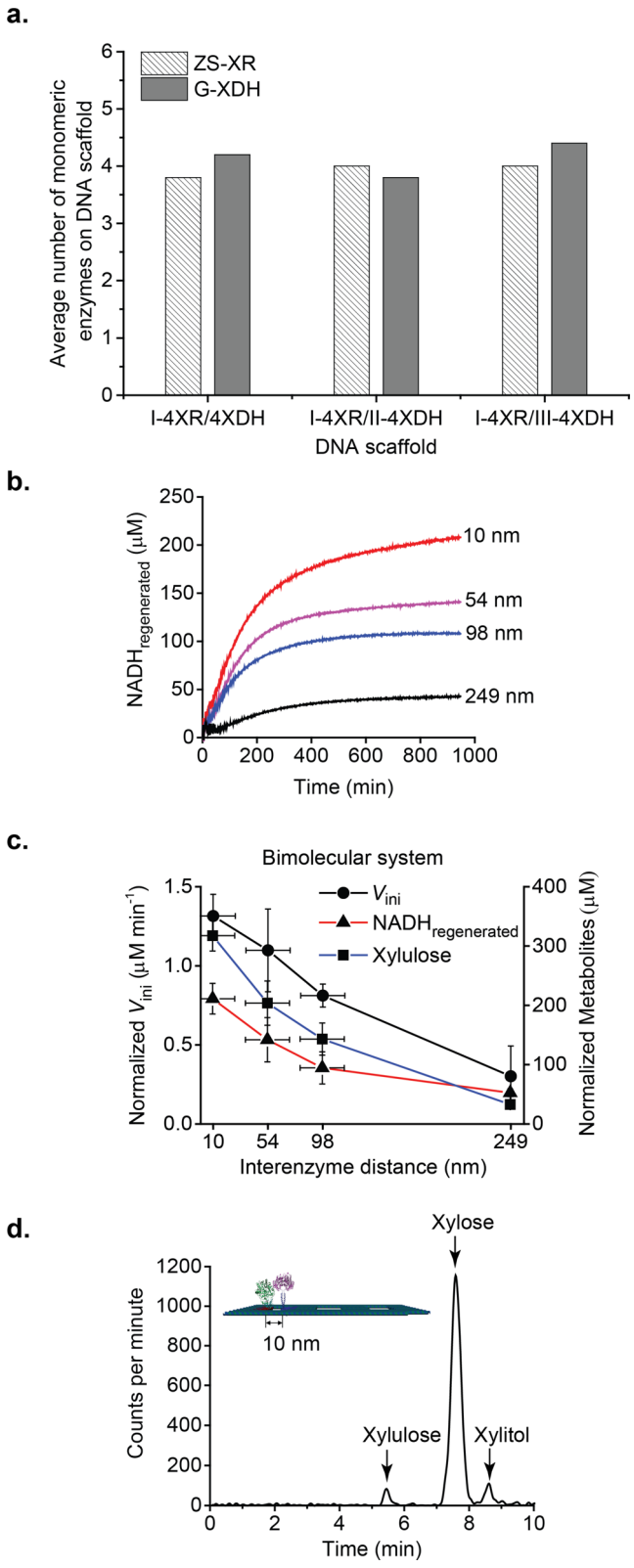

Figure 4. Analysis of enzyme cascade reactions for bimolecular diffusion. (a) The actual average numbers of ZS-XR and G-XDH monomer on the DNA scaffolds were estimated from frequency distributions of molecular volumes for each enzyme (Figures S12–S14 in the Supporting Information). (b) Time-course profiles of the amount of NADH regenerated by G-XDH when the enzymes were coassembled with interenzyme distances of 10, 54, and 98 nm and for the free diffusion system, in which ZS-XR was located on the DNA scaffold (21 nM) while the second enzyme G-XDH (85 nM) was

DOI: 10.1021/jacs.5b10198
J. Am. Chem. Soc. 2016, 138, 3012–3021

Figure 4. continued

present in free solution (theoretically estimated interenzyme distance of 249 nm). (c) Plots of the normalized V_{ini}, the normalized amount of regenerated NADH, and the normalized amount of xylulose produced after 16 h against the interenzyme distances. (d) The production of xylitol and xylulose was analyzed using HPLC chromatograms of the reaction mixture after a 16-h incubation with [1-^{3}H]xylose. The interenzyme distance was 10 nm. Error bars of the *y*-axis were generated as the standard deviation of the mean from at least three replicates. Error bars of the *x*-axis indicated plausible ranges of the motion of ZS-XR and G-XDH bound to the target sequences, which were estimated by the molecular modeling analyses (Figure S11 in the Supporting Information).

under steady-state conditions (after 16 h). As described above, when both of the enzymes were coassembled in a distance-dependent manner, the actual number of each enzyme attached on the DNA scaffold varied with the interenzyme distance (Figure 4a and Figures S12−S14 in the Supporting Information); this may reflect the yield of NADH regeneration. To avoid any discrepancies in the cascade reactions due to the yield of coassembly, the V_{ini} and the amount of regenerated NADH were normalized (the detail was shown in Note S4 in the Supporting Information). The normalized V_{ini} and the normalized amount of regenerated NADH were plotted against the interenzyme distance, as shown in Figure 4c. Both the normalized V_{ini} and the normalized amount of regenerated NADH decreased gradually with the increase in the interenzyme distance.

To further confirm the efficiency of the cascade reaction depending on the interenzyme distance, the yield of the final product xylulose was determined by HPLC using [1-^{3}H]xylose as the substrate (Figure 4d and Figure S16 and Table S3 in the Supporting Information). The normalized amount of xylulose after 16 h was also plotted against the interenzyme distance (Figure 4c and Table S4 in the Supporting Information). The formation of xylulose was decreased as the interenzyme distance increased, and the normalized amount of xylulose was much higher than that obtained for the reaction with the free diffusion system (Figure 4c and Table S4 in the Supporting Information). Taken together, these results suggested that the bimolecular transport of xylitol and NAD^+ occurred efficiently for the enzymes coassembled on the DNA scaffold and that the efficiency of this cascade reaction was in inverse proportion to the interenzyme distance. The sequential enzymatic reaction system assembled on the DNA scaffold also allowed us to evaluate the regeneration of the NADH cofactor.

The distance dependency of the three-dimensional (3D) diffusion of xylitol and NAD^+ was evaluated using Brownian motion (Note S5 and Figure S18 in the Supporting Information). Our data showed that the diffusion of xylitol in water[52] was much faster than that of NAD^+.[53] On the basis of the trend of distance dependency of the cascade reaction in our bimolecular transport system (Figure 4c), it is reasonable to consider the 3D Brownian motion as a possible mechanism through which the intermediates transport to the second enzyme G-XDH.

To assess how the slow diffusion of NAD^+ alone affected the efficiency of the enzyme cascade, the reactions were evaluated with intentionally added xylitol. In the presence of excess amounts of substrates for both the enzymes and the NADH cofactor for the first enzyme ZS-XR, the efficiency of the enzyme cascade will depend exclusively on the transport of NAD^+. Except for the presence of xylitol, the same concentrations of enzyme assemblies were applied to compare the distance effect between bimolecular (NAD^+ and xylitol) and unimolecular (NAD^+) transport systems. The time-dependent changes in the absorbance of NADH were measured, and the amount of regenerated NADH was estimated after 16 h (Figure S17 in the Supporting Information). The normalized V_{ini} and the normalized amount of regenerated NADH were plotted against the interenzyme distances (Figure 5a and Table S5 in

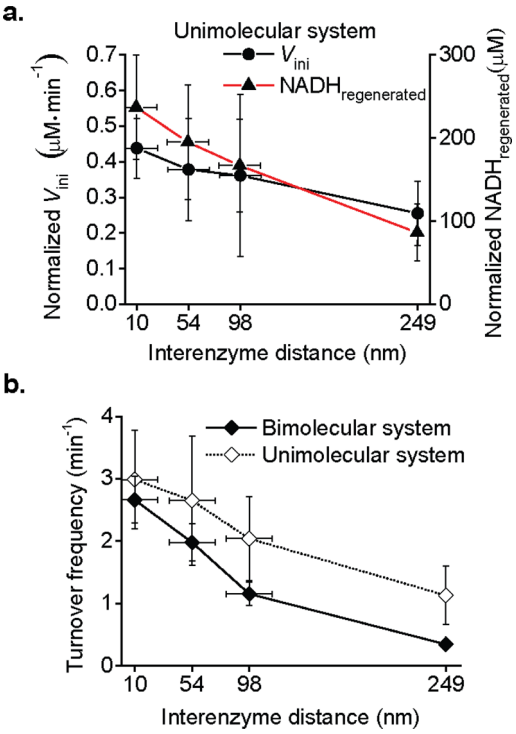

Figure 5. Analysis of enzyme cascade reactions for unimolecular diffusion and comparison with bimolecular diffusion. The enzyme cascade reactions for unimolecular diffusion were conducted for the enzymes coassembled with interenzyme distances of 10, 54, and 98 nm and for the free diffusion system, in which ZS-XR was located on the DNA scaffold (21 nM) while the second enzyme G-XDH (85 nM) was present in free solution (with a theoretically estimated interenzyme distance of 249 nm, the same as the bimolecular diffusion system). (a) Plots of the normalized V_{ini} and the normalized amount of regenerated NADH after 16 h against interenzyme distances for the unimolecular (NAD^+) transport. (b) Plots of the turnover frequencies for the uni- and bimolecular transport systems. Experimental conditions are shown in the Materials and Methods. Error bars of the *y*-axis were generated as the standard deviation of the mean from at least three replicates. Error bars of the *x*-axis indicated plausible ranges of the motion of ZS-XR and G-XDH bound to the target sequences, which were estimated by the molecular modeling analyses (Figure S11 in the Supporting Information).

the Supporting Information). There was a gradual decrease in the normalized amount of regenerated NADH when the interenzyme distance was increased from 10 to 249 nm (Note S3 in the Supporting Information). Overall, these plots showed a distance dependency similar to that observed for the bimolecular intermediate transport (Figure 4c). The results for the unimolecular NAD^+ transport system were in parallel with the previous studies on unimolecular H_2O_2 diffusion

DOI: 10.1021/jacs.5b10198
J. Am. Chem. Soc. 2016, 138, 3012−3021

between the GOx/HRP pair by Brownian motion on the DNA scaffold.[28−30]

In order to directly compare the distance dependency of diffusion processes for the unimolecular substrate, i.e., NAD^+ alone, and the bimolecular substrates, i.e., NAD^+ and xylitol, the turnover frequency[54−56] for each system was calculated from the normalized amount of regenerated NADH divided by the concentration of the second enzyme G-XDH on the DNA scaffold in the time unit.[57] Plots of turnover frequency against interenzyme distances (Figure 5b) revealed that the turnover frequency of the bimolecular transport system decreased with the increase of interenzyme distance. The ratios of turnover frequency at each interenzyme distance against that of the free diffusion condition were 9.0 (10 nm), 6.7 (54 nm), and 4.0 (98 nm). On the other hand, that of unimolecular transport was less sensitive to the increase of interenzyme distance. The ratios of turnover frequency at each interenzyme distance against that of the free diffusion condition were 2.6 (10 nm), 2.3 (54 nm), and 1.8 (98 nm). These results suggested that the transport of the bimolecular substrates xylitol and NAD^+ was more sensitive to the interenzyme distance than that of the unimolecular NAD^+, possibly reflecting the faster diffusion of xylitol over NAD^+.

DISCUSSION

To locate XR and XDH on the DNA scaffold, we applied their protein adaptor derivatives. ODN-conjugated enzymes were used for attachments on the DNA origami surface by other groups[28−31,35] and were found to decrease the enzyme activity when compared to the native enzymes. We were able to overcome this problem in the present study by applying DNA-binding protein adaptors. In fact, the recombinant enzymes conjugated with the protein adaptor were found to maintain or even enhance the activity when compared with the activity of the original enzyme. In addition to maintaining the activity of the enzyme, the assembly yield of the enzymes in close proximity is important. In our protein-adaptor-based method, we could successfully assemble the enzymes with a yield of 75% when the designed interenzyme distance was 10 nm, whereas in the ODN-conjugated enzyme strategy, this yield was about 45% when the enzymes were placed 10 nm apart.[29] It is particularly important to note that the actual number of assembled enzymes was often difficult to determine using the ODN-conjugated method,[29,30] in contrast, using our present method, the number of assembled enzymes was actually determined and controlled according to the number of adaptor binding sites. These results clearly indicated the advantages of our protein-adaptor-based methods for efficient loading of the enzymes on the DNA scaffold. Our method can be applied to construct various recombinant enzymes conjugated with the DNA binding adaptor by simply using the conventional protein engineering technique. Moreover, a single DNA origami could be used for distance-dependent analyses by changing the location of the binding site for the second enzyme, whereas in DNA strips reported by Wilner et al.,[28] a different scaffold design was necessary in order to create different interenzyme distances.

From our data, we could compare the mechanism through which the intermediates (here xylitol and NAD^+) were transported from one enzyme to another on the DNA scaffold with the mechanisms proposed in previous reports of the enzyme cascade of glucose oxidase (GOx) and horseradish peroxidase (HRP),[28−31] in which hydrogen peroxide (H_2O_2) is the sole intermediate. Fu et al.[29] simulated the 3D Brownian motion of the intermediate H_2O_2, and their results were consistent with the diffusion model for the intermediate transport from one enzyme to another when the interenzyme distances were 20 and 65 nm. However, at the interenzyme distance of 10 nm, the cascade activity suddenly increased (more than 15-fold) compared with that of the unassembled enzymes. These data suggested that the formation of a hydration layer around the protein constrained its translational and rotational degrees of freedom, leading to a dimensionally limited diffusion mechanism that dominated over 3D diffusion. In contrast, reports by Wilner et al.[28] and Fu et al.,[30] using the same GOx/HRP pair, indicated that the cascade activity was gradually decreased as the interenzyme distance increased from 5 to 45 nm. Indeed, the distance between the two enzymes played a major role in the efficiency of the cascade reactions, as previously reported.[6,13,14,28−31,35,51] We tested the interenzyme distances of 10, 54, and 98 nm and found that the efficiency was highest when the enzymes were placed at a distance of 10 nm. Analysis of the initial reaction rate, regenerated amount of NADH, and simulation of the intermediates' diffusion indicated that the intermediates diffused to the second enzyme by Brownian motion. The efficiency of cascade reaction by coassembled enzyme was enhanced over that in the bulk solution when the enzymes were located within the average interenzyme distance determined by the concentration of freely diffused enzymes, in accordance with the local concentration gradient of the intermediates between enzymes. This notion was also supported by the result of the concentration dependency on the efficiency of the cascade reaction (Note S6, Figure S19, and Table S6 in the Supporting Information).

One of the most important aspects of this study was our analysis of the simultaneous transport of both the substrate xylitol and the cofactor NAD^+. In previous studies, either the substrate alone or the cofactor alone was diffused from the first enzyme to the second enzyme.[28−31,35] Our investigation suggested that interenzyme distance had a greater effect on the efficiency of the cascade enzyme reaction when bimolecular transport occurred, further supporting the importance of the spatially controlled assembly of the two enzymes during the design of the artificial cascade.

The stoichiometry of enzymes in the cascade could also be a critical factor in determining the efficiency of the natural metabolic cascade reaction.[6,13−15] Our artificial enzyme cascade would be useful to investigate the effects of the ratio of the downstream enzyme (G-XDH) to the upstream enzyme (ZS-XR) within the cascade by simply varying the number of adaptor binding sites. In addition, because the enzymes were assembled on the 2D DNA scaffold in this study, minimal enhancement of the cascade reaction should have been observed. Application of 3D scaffolds designed by DNA origami with the interenzyme distances found in this study would further enhance metabolic cascade reactions. In summary, our mechanistic investigation of biomolecular transport provided important insights into the fundamental understanding of metabolic cascade reactions. This investigation will be helpful for further development of various other scaffold-assisted assemblies of biologically important enzymes using predesigned patterns to achieve artificial enzymatic cascade reactions with higher yield.

CONCLUSIONS

In this study, we designed and constructed a sequential enzymatic reaction system based on the D-xylose metabolic pathway in the cavity of the DNA scaffold. The first two

DOI: 10.1021/jacs.5b10198
J. Am. Chem. Soc. 2016, 138, 3012−3021

enzymes in this pathway, XR and XDH, were located in the cavity of the DNA scaffold at predesigned positions in a distance-dependent manner. Our results showed that this reaction system, which localized the two enzymes in close proximity to facilitate transport of reaction intermediates, resulted in significantly higher yields of the product and allowed for recycling of cofactors. The efficiency of the cascade reaction with the biomolecular transport of xylitol and NAD^+ depended more on the interenzyme distance than that of the cascade reaction with unimolecular transport between two enzymes. By using our protein-adaptor-based method for efficient loading of the enzymes on the DNA scaffold and their volume analysis, the number of assembled enzymes was determined and controlled according to the number of adaptor binding sites. This advantage of our method would be useful to investigate further the effects of the ratio of enzymes within the cascade, which could be a critical factor in determining the enzyme cascade reaction. Our investigation helps further development of various scaffold-assisted assemblies of biologically important enzymes with predesigned patterns to achieve efficient natural or artificial enzymatic cascade reactions.

MATERIALS AND METHODS

Materials. The single-stranded M13mp18 viral DNA and restriction enzymes (*Nde*I and *Hind*III) were purchased from New England Biolabs. Purified DNA origami staple strands, oligonucleotide primers, and all other oligonucleotides were obtained from Sigma-Aldrich (St. Louis, MO) or Gene Design Inc. (Osaka, Japan). *Escherichia coli* BL21(DE3)pLysS competent cells were purchased from Invitrogen (Carlsbad, CA). β-Nicotinamide adenine dinucleotide in reduced (NADH) and oxidized (NAD^+) forms were obtained from Oriental Yeast (Tokyo, Japan). COSMOSIL packed column sugar-D (4.6 i.d. × 250 mm) and HPLC-grade acetonitrile were purchased from Nacalai Tesque (Kyoto, Japan). Xylose, xylitol, xylulose, gel electrophoresis grade acrylamide, bis(acrylamide), phenol, and all other chemicals and reagents were purchased from Wako Chemicals (Tokyo, Japan) or Nacalai Tesque (Kyoto, Japan). [1-^{3}H]Xylose was from American Radiolabeled Chemicals Inc. (St. Louis, MO). Mini Elute Gel Extraction Kit was from QIAGEN (Tokyo, Japan). HiTrap SP XL column (5 mL), HisTrap HP column (5 mL), HiTrap Q HP column (5 mL), and Sephacryl S-400 were purchased from GE Healthcare Japan Inc. (Tokyo, Japan). PrimeSTAR HS DNA polymerase, T4 DNA ligase, and *E. coli* DH5α competent cells were obtained from TaKaRa Bio Inc. (Shiga, Japan). Ultrafree-MC-DV was obtained from Merckmillipore (Darmstadt, Germany). A buffer (pH 7.6 or 7.0) containing 40 mM Tris-HCl, 20 mM acetic acid, and 12.5 mM $MgCl_2$ was used unless otherwise designated.

Construction of a Vector for ZS-XR. A NADH-selective mutant of xylose reducase (XR) in *YEpM4* vector (provided from Dr. Tsutomu Kodaki)[46] and ZS in *pET-30a-ZF-SNAP*[48] vector were amplified by PCR using the primer pairs shown in Table S9 in the Supporting Information, respectively. The PCR products were run on a 1% agarose gel in 1× TAE buffer and were purified by a Mini Elute Gel Extraction Kit. The PCR products and pET-30a were digested with *Nde*I and *Hind*III and were purified in the same manner, separately. These products were incubated with T4 DNA ligase. The mixture was transformed into *E. coli* DH5α competent cells for amplification. Then the purity and sequence of vector encoding ZS-XR (termed as *pET-30a-ZS-XR*) were checked and transformed into *E. coli* BL21(DE3)pLysS competent cells.

Overexpression and Purification of ZS-XR. The transformed cells were grown at 37 °C until OD_{600} reached 0.5, and protein expression was induced with 1 mM IPTG for 24 h at 25 °C. The soluble fraction of the cell lysate containing ZS-XR was loaded on a HisTrap HP column in 50 mM phosphate buffer (pH 7.0) containing 200 mM NaCl, 5 mM mercaptoethanol, and 10 mM xylose and was eluted by imidazole gradient. The main fractions containing ZS-XR were loaded on a HiTrap SP XL column in 20 mM phosphate buffer (pH 7.0) containing 5 mM mercaptoethanol and 10 mM xylose and eluted by NaCl gradient. The main fractions containing ZS-XR were loaded on a HiTrap Q HP column (conditions: pH 7.0, 20 mM phosphate buffer containing, 5 mM mercaptoethanol, and 10 mM xylose) and eluted by NaCl gradient. The purified ZS-XR was dialyzed by using 50 mM phosphate buffer (pH 6.0), containing 0.2 M NaCl, 5 mM mercaptoethanol, 50 μM $ZnCl_2$, and 10 mM xylose, and 50% glycerol and stocked at −20 °C. The purity of ZS-XR was checked by SDS−polyacrylamide gel electrophoresis (PAGE). The major band in SDS−PAGE (Figure S2a in the Supporting Information) corresponded to the calculated molecular weight of ZS-XR (69 631) with purity over 95%. The amino acid sequence of ZS-XR is shown in Figure S2b in the Supporting Information.

Preparation of the DNA Scaffold with Three Cavities. A solution (50 μL) containing M13mp18 single-stranded DNA (10 nM) and staple DNA strands (5 equiv, 50 nM; all of staple strands sequences are shown in Tables S10−S12 in the Supporting Information) in a buffer (pH 7.0) was heated at 95 °C for 1 min, incubated at 53 °C for 30 min, and then cooled down to 4 °C by using a thermal cycler (C1000 Thermal Cycler, BioRad). The sample was purified by gel filtration (400 μL volume of Sephacryl S-400) in Ultrafree-MC-DV with a buffer (pH 7.0). The purity and recovery rate of the DNA scaffold was analyzed by agarose gel electrophoresis (Figure S5 in the Supporting Information). Then, the solution containing the purified DNA scaffold was concentrated by lyophilization. The concentration of DNA scaffold was quantified by absorbance at 260 nm (described in detail in Note S1 of the Supporting Information). The schematic structures of DNA scaffold used in this study are shown in Figure S4 in the Supporting Information.

Preparation of the DNA Scaffold Assembled with ZS-XR and/or G-XDH. Each of the concentrated DNA scaffolds containing either the binding sites with BG modification for ZS-XR and/or the binding sites for G-XDH was incubated with ZS-XR and/or G-XDH in a buffer (pH 7.0) containing 1 mM DTT under the conditions shown in the caption of figures or tables. The mixture was purified by gel filtration (400 μL volume of Sephacryl S-400 in Ultrafree-MC-DV with a buffer, pH 7.0) to remove the excess amount of unbound enzymes. Effective removal of the unbound enzymes was demonstrated in Figure S10 (Supporting Information) and in our previous report.[42] The fractions containing DNA scaffold were utilized for AFM analysis or enzymatic assay. The detail of the determination of the concentration is described in Note S1 of the Supporting Information.

AFM Imaging. The sample was deposited on a freshly cleaved mica (5 or 1.5 mm ϕ) surface, adsorbed for 5 min at ambient temperature, and then washed three times with a buffer (pH 7.0). The sample was scanned in tapping mode using a MultiMode microscope (Bruker) equipped with a Nanoscope V controller or a silicon nitride cantilever (Olympus BL-AC40TS-C2) or using a fast-scanning AFM system (Nano Live Vision, RIBM Co. Ltd., Tsukuba, Japan) with a silicon nitride cantilever (Olympus BL-AC10DS-A2).

Statistical Analysis of AFM Images. At least three independent preparations of each sample were analyzed by AFM and several images were acquired from different regions of the mica surface. The total number of DNA scaffold corresponds to the number of expected rectangular shapes possessing three cavities observed by AFM. The specific and nonspecific binding of ZS-XR or G-XDH was counted for only ZS-XR or G-XDH bound to the perfectly folded DNA scaffold. The details of analytical process are shown below.

Yield of DNA-Scaffold-Assembled ZS-XR or G-XDH. The yield of ZS-XR on DNA scaffold ($P_{specific}$) was calculated as the percentage of the number of modified DNA scaffolds bearing ZS-XR at the expected position ($N_{expected\ posi}$), e.g., cavity I in the case of I-4XR/II-4XDH, over the total number of well-formed DNA scaffold (N_{total}):

$$P_{specific} = (N_{expected\ posi}/N_{total}) \times 100$$

The yield of ZS-XR that existed at the unexpected positions ($P_{nonspecific}$) was calculated as the percentage of cavities modified nonspecifically by ZS-XR ($N_{unexpected\ posi}$), e.g., cavity II or III in the

DOI: 10.1021/jacs.5b10198
J. Am. Chem. Soc. 2016, 138, 3012−3021

case of I-4XR/II-4XDH, over the total number of cavities (e.g., positions II and III in the case of I-4XR/II-4XDH) of well-formed DNA scaffold ($2N_{total}$):

$$P_{nonspecific} = (N_{unexpected\ posi}/2N_{total}) \times 100$$

$P_{specific}$ and $P_{nonspecific}$ for G-XDH were calculated in a similar manner.

Yield of DNA Scaffold with Coassembled ZS-XR and G-XDH. Prior to determine the yield of coassembled ZS-XR and G-XDH on the DNA scaffold, the yield of assembled ZS-XR on the DNA scaffold was calculated as described above.

The yield of coassembled ZS-XR and G-XDH on DNA scaffold ($P_{coassembly}$) was calculated as the percentage of the number of modified DNA scaffolds bearing the two enzymes (ZS-XR and G-XDH) at the expected position on the DNA scaffold ($N_{expected\ posi}$) over the total number of well-formed DNA scaffold (N_{total}):

$$P_{coassembly} = (N_{expected\ posi}/N_{total}) \times 100$$

The yield of ZS-XR and/or G-XDH found in nonspecific positions ($P_{nonspecific}$) was calculated as the percentage of the number of cavities modified nonspecifically by ZS-XR and/or G-XDH ($N_{unexpected\ posi}$) over the total number of cavities of well-formed DNA scaffold (N_{total}):

I-4XR/4XDH: $P_{nonspecific} = (N_{unexpected\ posi}/2N_{total}) \times 100$

I-4XR/II-4XDH or I-4XR/III-4XDH:

$$P_{nonspecific} = (N_{unexpected\ posi}/N_{total}) \times 100$$

Volume Analysis of AFM Images. For volume analysis, the AFM images were taken by using a high-speed AFM system (Nano Live Vision, RIBM Co. Ltd., Tsukuba, Japan) with a silicon nitride cantilever (Olympus BL-AC10DS-A2). The volume of ZS-XR or G-XDH located inside the cavity of the DNA scaffold was analyzed by using SPIP software (ver. 6.2.8, Image Metrology) and the *Z* material volume value, defined as the volume of all the pixels inside the shape's contour with the Z value used. The volume data were displayed as a histogram plot and fractions were analyzed by means of a nonlinear curve fit by Origin (ver. 9.1) software. The molecular volumes were converted to the number of enzyme molecules by using standard curves (Figures S6 and S7 and as described in Note S2 of the Supporting Information.

Enzyme Assay of ZS-XR (or XR). Catalytic activity of ZS-XR (or mutant XR) was analyzed according to the previously reported methods with slight modifications[6,47] by measuring the changes of absorbance at 340 nm (25 °C) derived from the oxidation of NADH with an Infinite 200 PRO microplate reader (TECAN Austria GmbH). In a typical experiment, a reaction was started with an addition of NADH (0.15 mM) to a mixture of ZS-XR (25 nM) and xylose (200 mM) in a buffer (pH 7.0) containing 100 mM NaCl, 1 μM $ZnCl_2$, and 0.02% Tween-20. The kinetic parameters K_m and k_{cat} of ZS-XR for NADH or xylose were determined by Lineweaver–Burk plots, as shown in Table S6 in Supporting Information. The production of xylitol in the reaction containing [1-^{3}H]xylose (200 nM) and nonlabeled xylose (200 mM) was determined by HPLC. The HPLC conditions were as follows: COSMOSIL parked column sugar-D (4.6 i.d. × 250 mm) with isocratic elution solvent (acetonitrile:water = 80:20); flow rate, 1 mL/min; column temperature, 30 °C; detected by radiodetectors (β-RAM 5C Lablogic).

Enzyme Assay of G-XDH. The catalytic activity of G-XDH was analyzed as described previously.[46] The kinetic parameters K_m and k_{cat} of G-XDH for NAD^+ or xylitol were determined by Lineweaver–Burk plots as shown in Table S7 in the Supporting Information.

Enzyme Assays in the Presence of Both ZS-XR and G-XDH. In the bimolecular intermediates' (xylitol and NAD^+) transport system, the reaction was started with an addition of NADH (2 mM) to a mixture of ZS-XR and/or G-XDH located on the DNA scaffold (21 nM) and xylose (12.5 mM) in a buffer (pH 7.0) containing 100 mM NaCl, 1 μM $ZnCl_2$, and 0.02% Tween-20, and the progress of reaction was monitored by measuring the time-course changes of absorbance at 340 nm. The production of xylitol and xylulose from [1-^{3}H]xylose (200 nM) was analyzed by HPLC as described above. For the unimolecular (NAD^+) transport reaction system, the reaction conditions of bimolecular system, except for the presence of xylitol (300 mM), were applied. The processes to normalize the initial rate of NADH regeneration and the amount of products are described in Note S4 of the Supporting Information. The turnover frequency for each system was calculated from the normalized amount of products divided by the concentration of the second enzyme G-XDH on DNA scaffold in the time unit.

■ ASSOCIATED CONTENT

Supporting Information

The Supporting Information is available free of charge on the ACS Publications website at DOI: 10.1021/jacs.5b10198.

Molecular models (Figure S1), preparation (Figure S2), and evaluation of the activity (Figure S3, Tables S1, S7, S8) of the adaptor modified enzymes; structures of the DNA origami scaffolds (Figure S4); estimating the concentration of DNA origami and DNA origami–protein complexes (Note S1 and Figure S5); statistical analyses of AFM images for determining the occupancies of DNA scaffolds by enzymes (Table S2); estimating the actual number of ZS-XR and G-XDH molecules bound to the specific sites on the DNA scaffold (Note S2, Figures S6–S8, S12–14); effect of the DNA scaffold on the activity of ZS-XR (Figure S9); effective removal of the unbound ZS-XR upon purification of the ZS-XR-bound DNA scaffold (Figure S10); calculation of the interenzyme distance (Note S3, Figure S11); normalization of time-course reaction profiles (Note S4, Figures S15, S17, Tables S4, S5); HPLC analyses of the metabolites (Figure S16, Table S3); intermediates' diffusion model (Note S5, Figure S18); concentration-dependent experiment (Note S6, Figure S19, Table S6); nucleotide sequences of primers (Table S8) and staple strand DNAs used for the assembly of the DNA origami scaffolds (Tables S10–S12) (PDF)

■ AUTHOR INFORMATION

Corresponding Author

*t-morii@iae.kyoto-u.ac.jp

Notes

The authors declare no competing financial interests.

■ ACKNOWLEDGMENTS

The authors are grateful to Prof. Tsutomu Kodaki for providing the vectors encoding the enzymes. The authors thank Drs. Isao Saito and Arivazhagan Rajendran for helpful comments and discussions during the preparation of the manuscript. This work was supported in part by Grants-in-Aid for Scientific Research from the Ministry of Education, Culture, Sports, Science and Technology (Japan) to T.M. (nos. 25248038 and 15H01402) and E.N. (nos. 24651150 and 15H05492).

■ REFERENCES

(1) Welch, G. R. *Prog. Biophys. Mol. Biol.* **1978**, *32*, 103.
(2) Srere, P. A. *Annu. Rev. Biochem.* **1987**, *56*, 89.
(3) Welch, G. R.; Easterby, J. S. *Trends Biochem. Sci.* **1994**, *19*, 193.
(4) Spivey, H. O.; Ovádi, J. *Methods* **1999**, *19*, 306.
(5) Jørgensen, K.; Rasmussen, A. V.; Morant, M.; Nielsen, A. H.; Bjarnholt, N.; Zagrobelny, M.; Bak, S.; Møller, S. *Curr. Opin. Plant Biol.* **2005**, *8*, 280.

DOI: 10.1021/jacs.5b10198
J. Am. Chem. Soc. 2016, 138, 3012–3021

(6) Conrado, R. J.; Varner, J. D.; Delisa, M. P. *Curr. Opin. Biotechnol.* **2008**, *19*, 492.
(7) Lee, H.; Deloache, W. C.; Dueber, J. E. *Metab. Eng.* **2012**, *14*, 242.
(8) Zhang, Y. H. P. *Biotechnol. Adv.* **2011**, *29*, 715.
(9) Ricca, E.; Brucher, B.; Schrittwieser, J. H. *Adv. Synth. Catal.* **2011**, *353*, 2239.
(10) Good, M. C.; Zalatan, J. G.; Lim, W. A. *Science* **2011**, *332*, 680.
(11) Chen, A. H.; Silver, P. A. *Trends Cell Biol.* **2012**, *22*, 662.
(12) Schoffelen, S.; van Hest, J. C. M. *Soft Matter* **2012**, *8*, 1736.
(13) Agapakis, C. M.; Boyle, P. M.; Silver, P. *Nat. Chem. Biol.* **2012**, *8*, 527.
(14) Lee, J. W.; Na, D.; Park, J. M.; Lee, J.; Choi, S.; Lee, S. Y. *Nat. Chem. Biol.* **2012**, *8*, 536.
(15) Dueber, J. E.; Wu, G. C.; Malmirchegini, G. R.; Moon, T. S.; Petzold, C. J.; Ullal, A. V.; Prather, K. L. J.; Keasling, J. D. *Nat. Biotechnol.* **2009**, *27*, 753.
(16) Hirakawa, H.; Nagamune, T. *ChemBioChem* **2010**, *11*, 1517.
(17) You, C.; Myung, S.; Zhang, Y. H. P. *Angew. Chem., Int. Ed.* **2012**, *51*, 8787.
(18) Marguet, M.; Bonduelle, C.; Lecommandoux, S. *Chem. Soc. Rev.* **2013**, *42*, 512.
(19) Niemeyer, C. M.; Koehler, J.; Wuerdemann, C. *ChemBioChem* **2002**, *3*, 242.
(20) Erkelenz, M.; Kuo, C. H.; Niemeyer, C. M. *J. Am. Chem. Soc.* **2011**, *133*, 16111.
(21) Delebecque, C. J.; Lindner, A. B.; Silver, P. A.; Aldaye, F. A. *Science* **2011**, *333*, 470.
(22) Elcock, A. H.; Huber, G. A.; McCammon, J. A. *Biochemistry* **1997**, *36*, 16049.
(23) Ouporov, I. V.; Knull, H. R.; Huber, A.; Thomasson, K. A. *Biophys. J.* **2001**, *80*, 2527.
(24) Bauler, P.; Huber, G.; Leyh, T.; McCammon, J. A. *J. Phys. Chem. Lett.* **2010**, *1*, 1332.
(25) Idan, O.; Hess, H. *ACS Nano* **2013**, *7*, 8658.
(26) Eun, C.; Kekenes-Huskey, P. M.; Metzger, V. T.; McCammon, J. A. *J. Chem. Phys.* **2014**, *140*, 105101.
(27) Castellana, M.; Wilson, M. Z.; Xu, Y.; Joshi, P.; Cristea, I. M.; Rabinowitz, J. D.; Gitai, Z.; Wingreen, N. S. *Nat. Biotechnol.* **2014**, *32*, 1011.
(28) Wilner, O. I.; Weizmann, Y.; Gill, R.; Lioubashevski, O.; Freeman, R.; Willner, I. *Nat. Nanotechnol.* **2009**, *4*, 249.
(29) Fu, J.; Liu, M.; Liu, Y.; Woodbury, N. W.; Yan, H. *J. Am. Chem. Soc.* **2012**, *134*, 5516.
(30) Fu, Y.; Zeng, D.; Chao, J.; Jin, Y.; Zhang, Z.; Liu, H.; Li, D.; Ma, H.; Huang, Q.; Gothelf, K. V.; Fan, C. *J. Am. Chem. Soc.* **2013**, *135*, 696.
(31) Xin, L.; Zhou, C.; Yang, Z.; Liu, D. *Small* **2013**, *9*, 3088.
(32) Seeman, N. C. *Nature* **2003**, *421*, 427.
(33) Rothemund, P. W. K. *Nature* **2006**, *440*, 297.
(34) Douglas, S. M.; Dietz, H.; Liedl, T.; Högberg, B.; Graf, F.; Shih, W. M. *Nature* **2009**, *459*, 414.
(35) Fu, J.; Yang, Y. R.; Johnson-Buck, A.; Liu, M.; Liu, Y.; Walter, N. G.; Woodbury, N. W.; Yan, H. *Nat. Nanotechnol.* **2014**, *9*, 531.
(36) Timm, C.; Niemeyer, C. M. *Angew. Chem., Int. Ed.* **2015**, *54*, 6745.
(37) Fu, J.; Liu, M.; Liu, Y.; Yan, H. *Acc. Chem. Res.* **2012**, *45*, 1215.
(38) Meyer, R.; Giselbrecht, S.; Rapp, B. E.; Hirtz, M.; Niemeyer, C. M. *Curr. Opin. Chem. Biol.* **2014**, *18*, 8.
(39) Pavletich, N. P.; Pabo, C. O. *Science* **1991**, *252*, 809.
(40) Ellenberger, T. E.; Brandl, C. J.; Struhl, K.; Harrison, S. C. *Cell* **1992**, *71*, 1223.
(41) Nakata, E.; Liew, F. F.; Uwatoko, C.; Kiyonaka, S.; Mori, Y.; Katsuda, Y.; Endo, M.; Sugiyama, H.; Morii, T. *Angew. Chem., Int. Ed.* **2012**, *51*, 2421.
(42) Ngo, T. A.; Nakata, E.; Saimura, M.; Kodaki, S.; Morii, T. *Methods* **2014**, *67*, 142.
(43) Winkelhausen, E.; Kuzmanova, S. *J. Ferment. Bioeng.* **1998**, *86*, 1.
(44) Ngo, T. A.; Nguyen, T. H.; Bui, H. T. V. *Renewable Energy* **2012**, *37*, 174.
(45) Jeffries, T. W. *Curr. Opin. Biotechnol.* **2006**, *17*, 320.
(46) Watanabe, S.; Abu Saleh, A.; Pack, S. P.; Annaluru, N.; Kodaki, T.; Makino, K. *Microbiology* **2007**, *153*, 3044.
(47) Watanabe, S.; Kodaki, T.; Makino, K. *J. Biol. Chem.* **2005**, *280*, 10340.
(48) Nakata, E.; Dinh, H.; Ngo, T. A.; Saimura, M.; Morii, T. *Chem. Commun.* **2015**, *51*, 1016.
(49) Keppler, A.; Gendreizig, S.; Gronemeyer, T.; Pick, H.; Vogel, H.; Johnsson, K. *Nat. Biotechnol.* **2002**, *21*, 86.
(50) Moehlenbrock, M. J.; Toby, T. K.; Pelster, L. N.; Minteer, S. D. *ChemCatChem* **2011**, *3*, 561.
(51) Lin, J. L.; Palomec, L.; Wheeldon, I. *ACS Catal.* **2014**, *4*, 505.
(52) Lebeau, T.; Jouenne, T.; Junter, G. A. *Enzyme Microb. Technol.* **1998**, *22*, 434.
(53) Damian, A.; Omanovic, S. *J. Mol. Catal. A: Chem.* **2006**, *253*, 222.
(54) Boudart, M.; Djéga-Mariadassou, G. *Kinetics of Heterogeneous Catalytic Reactions*; Princeton University Press: Princeton, NJ, 1984.
(55) Spivey, J. J.; Roberts, G. W.; Goodwin, J. G., Jr.; Kim, S.; Rhodes, W. D. *Catalysis* **2006**, *17*, 320.
(56) Boudart, M. *Chem. Rev.* **1995**, *95*, 661.
(57) Kumar, B.; Llorente, M.; Froehlich, J.; Dang, T.; Sathrum, A.; Kubiak, C. P. *Annu. Rev. Phys. Chem.* **2012**, *63*, 541.

DOI: 10.1021/jacs.5b10198
J. Am. Chem. Soc. 2016, 138, 3012−3021